Ammonia-Rich High-Temperature Superconducting Intercalates of Iron Selenide Revealed through Time-Resolved in Situ X-ray and Neutron Diffraction
— Source link ↗

Stefan J. Sedlmaier, Simon J. Cassidy, Richard G. Morris, Michael Drakopoulos ...+6 more authors

Institutions: University of Oxford, Rutherford Appleton Laboratory

Topics: Selenide and Neutron diffraction

Related papers:

- Enhancement of the superconducting transition temperature of FeSe by intercalation of a molecular spacer layer

- Enhancement of superconducting transition temperature of FeSe by intercalation of a molecular spacer layer

- Superconductivity in the PbO-type structure α-FeSe

- Observation of superconductivity at 30~46K in AxFe2Se2 (A = Li, Na, Ba, Sr, Ca, Yb, and Eu)

- Observation of superconductivity at 30 K~46 K in AxFe2Se2 (A = Li, Na, Ba, Sr, Ca, Yb, and Eu)

Share this paper:

View more about this paper here: https://typeset.io/papers/ammonia-rich-high-temperature-superconducting-intercalates-dhnz2ujzk3

Ammonia-rich high temperature superconducting intercalates of iron selenide revealed through time-resolved *in-situ* X-ray and neutron diffraction.

Stefan J Sedlmaier,[1] Simon J Cassidy,[1,2] Richard G Morris,[1] Michael Drakopoulos,[2] Christina Reinhard,[2] Saul J Moorhouse,[1,2] Dermot O'Hare,[1] Pascal Manuel,[3] Dmitry Khalyavin[3] and Simon J Clarke[1*]

[1]*Department of Chemistry, University of Oxford, Inorganic Chemistry Laboratory, South Parks Road, Oxford, OX1 3QR, UK.* [2]*Diamond Light Source Ltd., Harwell Science and Innovation Campus, Didcot, OX11 0DE, UK .*[3]*ISIS Facility, STFC Rutherford Appleton Laboratory, Harwell Oxford, Didcot OX11 0QX, United Kingdom.*

Supporting Information Placeholder

ABSTRACT: The development of a technique for following *in-situ* the reactions of solids with alkali metal/ammonia solutions, using time-resolved X-ray diffraction methods, reveals high temperature superconducting ammonia-rich intercalates of iron selenide which reversibly absorb and desorb ammonia around ambient temperatures.

Iron-based superconductors exhibit rich chemistry and physics. Control of the transition between itinerant antiferromagnetism and superconductivity in several iron arsenides, selenides and phosphides is possible using applied pressures and isovalent or aliovalent substitutions to tune structural parameters and/or electron count. Understanding these materials' superconducting and magnetic properties may shed light on the behaviour of other classes of high temperature superconductor. Recent reviews describe developments in synthesis,[1] structure-property relationships,[2] materials properties[3] and theory.[4]

The tetragonal layered polymorph of FeSe is a superconductor[5] with a superconducting transition temperature (T_c) of 8.5 K for the composition $Fe_{1.01}Se$ (a small amount of intrinsic interstitial iron has a detrimental effect on superconductivity[6]). Ying *et al.*[7] revealed that solutions of alkali metals in liquid ammonia react with FeSe to produce intercalates with dramatically enhanced T_cs of up to 45 K. We showed,[8] in the case of the intercalates obtained from Li/ND_3 solutions, that the crystal structures of the products obtained after evaporation of the ammonia solvent and brief evacuation of the reaction vessels at room temperature are variants of the common $ThCr_2Si_2$ structure type with ND_3 and $[ND_2]^-$ moieties in sites 8-coordinate by selenide with N–D···Se hydrogen bonds. Li ions occupy sites coordinated by the ammonia or amide species and selenide (Figure 1, right). Scheidt *et al.* reported that amide-free materials may also be obtained.[9] The samples offer iron selenides with no iron vacancies and represent bulk variants of the minority phases which are presumed to be the source of superconductivity in $A_xFe_{2-y}Se_2$ samples (x ~0.8; y ~ 1.6; A = K, Rb, Cs) synthesised at high temperatures.[10,11] Ying *et al.*[12] report that ammonia may be completely removed from the intercalate $K_{0.3}(NH_3)_{0.7}Fe_2Se_2$ (T_c = 44 K) at 200 °C to yield a bulk superconducting phase $K_{0.3}Fe_2Se_2$ with the same T_c.

In this communication we describe a means to probe reactions using Powder X-ray Diffraction (PXRD) *in-situ* in liquid ammo-

nia at temperatures down to –78°C and reveal that the metal/ammonia intercalates described previously[7-9,12] are
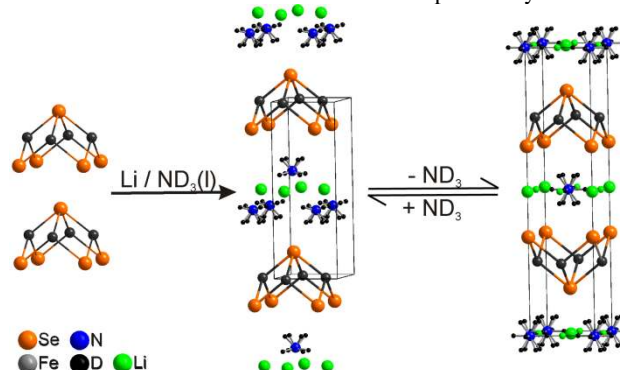

Figure 1. Schematic of the intercalation of lithium and ammonia into FeSe. The ammonia-rich intermediate is synthesised and described here; the structure and properties of the product of reversible ammonia desorption (right) is described in reference 8.

the decomposition products obtained, in the normal course of handling solid state compounds, from materials much richer in intercalated ammonia (Figure 1, center). The structure and properties of the ammonia-rich lithium/ammonia intercalate and its reversible adsorption and desorption of ammonia are described.

The syntheses of ammonia-rich FeSe intercalates were performed on the beamline, I12, at the Diamond Light Source, UK in an experiment conceived to investigate the intercalation *in-situ* and identify possible intermediate phases. For the reactions between Li/NH_3 solutions and FeSe, 4 mg (0.576 mmol) of Li metal were loaded, in an argon-filled glove box, into 18 mm o.d. × 4 mm wall pyrex ampoules sealed with teflon valves. 150 mg (1.113 mmol) of FeSe powder, synthesised from the elements as described previously,[8] was loaded into a side-arm projecting from the side of the ampoule so that it was not in contact with the alkali metal (see the Electronic Supporting Information (ESI)). The ampoule was connected to a Schlenk line, the end of the tube containing the alkali metal was placed in liquid nitrogen and around 5 cm³ of NH_3 were condensed onto the alkali metal. On melting the NH_3 ice at –78ºC in a CO_2/propan-2-ol cooling bath, the alkali metal dissolved to produce a blue solution. The ampoule was sealed and

transported to the beamline keeping the solution separate from the solid FeSe. The ampoules were either maintained with the end containing the solution in the CO_2/propan-2-ol slush, or were allowed to warm to room temperature (for safety precautions see the ESI). The ampoule was clamped to a remote-controlled stage with its rotation axis parallel and coincident with the X-ray beam. With the stirred Li/NH$_3$ solution exposed to a monochromatic 80 keV ($\lambda = 0.156$ Å) X-ray beam, diffractograms were measured continuously in time intervals of either 80 ms separated by a 40 ms dead time, or 4 s separated by a 1 s dead time with data collected using a Thales Pixium RF4343 flat panel detector. To initiate the reaction the ampoule was rotated about the beam direction so that the FeSe powder poured into the solution. The evolution of the diffraction pattern was monitored over a period of between a few minutes at ambient temperatures or a few hours at lower temperatures. This method is transferrable to other volatile solvent systems.
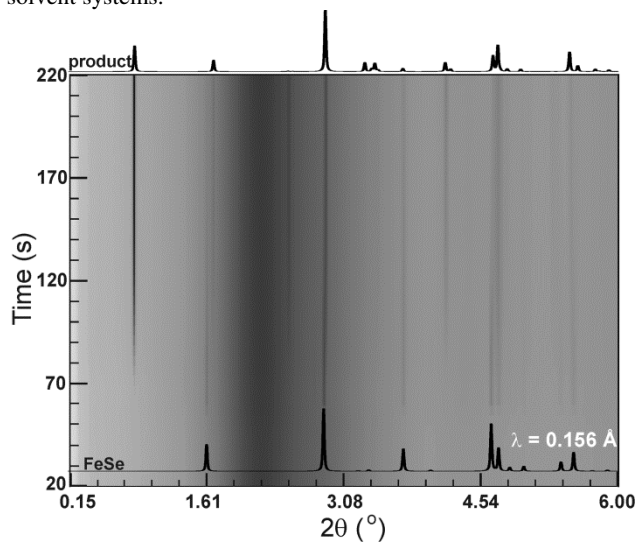

Figure 2. Film plot showing the evolution of the X-ray diffraction pattern measured on I12 when FeSe was added to Li/NH$_3$ solution at ambient temperature. Calculated diffractograms are shown for FeSe and the final product. (Further diffractograms (Figure S2) and a Rietveld analysis of the final product are shown in the ESI).

The *in-situ* PXRD measurements of the reaction between Li/NH$_3$ solutions and FeSe initially showed the appearance of reflections due to FeSe. At ambient temperature (Figure 2) these reflections rapidly diminished in intensity to be replaced by a new set of reflections. These new reflections bore a superficial resemblance to those of the *I*4/*mmm* Li/NH$_3$ intercalates of FeSe reported previously[8] in which the lowest angle Bragg peak is the (002) reflection with a *d*-spacing of about 8.5 Å, corresponding to the separation between adjacent Fe planes. However the product of these reactions probed *in-situ* had the lowest-angle Bragg peak at a *d*-spacing of 10.6 Å – 20 % larger than in the intercalates described previously. After about 2 min at ambient temperatures or 2.5 h at −78°C Bragg peaks due to FeSe had been completely replaced by those of the new material which is the final product of these intercalation reactions when the solid remains suspended in liquid ammonia.

For these reactions $\alpha(t)$ for a particular Bragg reflection (*hkl*) is defined as the temporal evolution of $I(t)/I(\text{max})$ for that reflection. For a reaction with no intermediate phases the intensity evolution of reactant and product Bragg peaks should cross at $\alpha = 0.5$, while a crossing at $\alpha < 0.5$ suggests the presence of an intermediate phase.[13] In the case of the lithiation reaction shown in Figure 2 there appears to be a seamless transition between FeSe and the new product. However, plots of $\alpha(t)$ for the (001) Bragg reflec-

tions of FeSe and the product (Figure S10), cross at $\alpha \sim 0.4$ at room temperature suggesting that an intermediate phase exists.

The room temperature diffractograms indeed revealed the presence of a crystalline intermediate phase (Figures S17 and S18), but the two observable reflections at *d*-spacings of 6.69 and 3.26 Å were insufficient to allow its identification. In low temperature reactions, by contrast, the normalized intensities of FeSe and product (001) Bragg reflections cross at $\alpha \sim 0.1$ (Figures S12, S14 & S16) and film plots (Figures S11, S13 & S15) show a period between the near-disappearance of the FeSe reflections and the appearance of reflections from the product when little crystalline material is present.[13]

For the final product of Li/NH$_3$ intercalation all reflections were indexed on a primitive tetragonal unit cell with refined room temperature lattice parameters $a = 3.82766(8)$ Å and $c = 10.5938(7)$ Å. Systematic absences were consistent with the space groups *P*4/*n* or *P*4/*nmm* and *ab initio* structure solution in *P*4/*nmm* using the charge flipping algorithm as implemented in TOPAS Academic[14] resulted in a structural model with FeSe layers stacked as in the starting material FeSe (which also crystallises in *P*4/*nmm*) but pushed apart, accommodating a double layer of light atoms (N atoms from the ammonia molecules) in the interlayer region. This is in contrast to the single layer of N atoms found in the case of the intercalates described previously.[8] This new model, with the PbFCl structure type (the "111" structure in the context of iron superconductors), gave an excellent Rietveld fit to the *in-situ* PXRD data (Figure S3, Tables S1 & S2).

Similar reactions with solutions of K and Rb in NH$_3$ revealed similar general behaviour: when PXRD measurements were performed *in-situ*, phases were identified with much longer lattice parameters perpendicular to the FeSe layers (Table 1) than the ammonia-poor intercalates described previously.[7,12] The unit cell volumes for K/NH$_3$ intercalates decrease as the K content increases which mirrors the observation by Ying *et al.* for the ammonia-poor K/NH$_3$ intercalates[12] and is presumably a consequence of an increased ionic bonding within the intercalate layers as the K$^+$ and amide content increases. The detailed crystal structures of the ammonia-poor and ammonia-rich K and Rb intercalates require further investigation.

Table 1. Lattice parameters and cell volumes of the final products of reactions of alkali metal/ammonia solutions with FeSe determined from I12 PXRD data (Figures S4–S6).

metal/FeSe ratio	a (Å)	c (Å)	V (Å^3)
Li/FeSe = 0.5	3.82766(8)	10.5938(7)	155.210(12)
K/FeSe = 0.15	3.8602(1)	10.1793(1)	151.7(12)
K/FeSe = 0.3	3.8348(5)	9.8492(3)	144.8(6)
Rb/FeSe = 0.5	3.8416(2)	10.0408(7)	148.2(19)

In order to fully describe the structure of the new Li/ammonia intercalate, a 1 g sample of the ammonia-poor intercalate Li$_{0.6}$(ND$_3$)$_{0.8}$(ND$_2$)$_{0.2}$Fe$_2$Se$_2$ was placed in a thin-walled 8 mm diameter cylindrical vanadium container and attached to the Schlenk line. The sample container was evacuated briefly, then cooled to −10 °C by means of an ice/salt bath and then exposed to 1 atm of ND$_3$ gas (99% D). After four hours the container was sealed, while cold, with a steel cap and an indium gasket under a stream of ND$_3$ gas. The mass change of the powder during loading suggested the absorption of approximately 1 mole of ND$_3$ per mole of Li$_{0.6}$(ND$_3$)$_{0.8}$(ND$_2$)$_{0.2}$Fe$_2$Se$_2$. Powder Neutron Diffraction (PND) data collected at 270 K on WISH at the ISIS Facility, UK revealed a diffraction pattern composed of a single phase consistent with the ammonia-rich intercalate obtained in the *in-situ* X-ray diffraction experiments (tetragonal P, $a = 3.81386(3)$ Å, $c = 10.5278(1)$ Å).
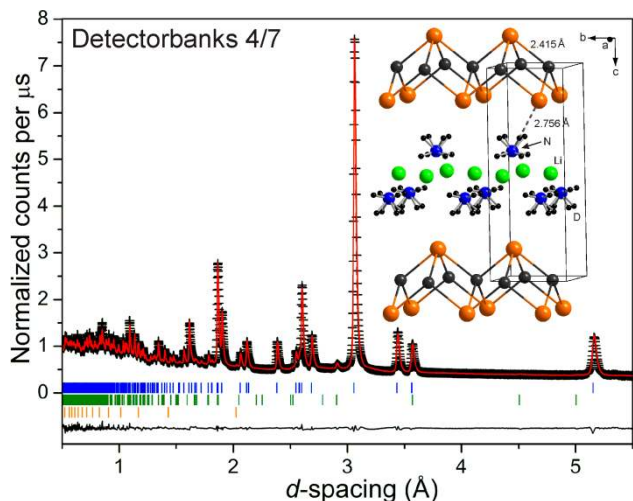
Figure 3. Observed (black crosses) and calculated (red line) neutron powder diffraction pattern and difference profile of the Rietveld refinement of the structure of the deuterated ammonia-rich Li/ND$_3$ intercalate against WISH data at 5 K and the final crystal structure; peak positions are marked by vertical lines (intercalate-blue (99.4 wt%), LiND$_2$-green (0.2 wt%), Fe-orange (0.4 wt%).

This confirms that compounds similar to those identified in the *in-situ* PXRD measurements can be regenerated by exposure of the ammonia-poor intercalates[8] to ammonia at low temperatures. PND measurements on a second sample which had been exposed to 1 atm of ND$_3$ at 0°C for four hours revealed a mixture of just the new ammonia-rich and the ammonia-poor[8] materials (see Figure S8) suggesting that absorption of further ammonia by the ammonia-poor material does not proceed via any other stable phase. A longer PND data collection at 5 K on the pure ND$_3$-rich intercalate (Figure 3) confirmed the partial structure derived from the *in-situ* X-ray diffraction experiments and enabled the D and Li atoms to be located. The refined structure ($P4/nmm$, $a = 3.79756(2)$, $c = 10.30704(8)$ Å at 5 K) is shown in Figure 3 and the refined parameters are supplied in Tables S3–S6. The refined composition of Li$_{0.6(1)}$(ND$_{2.7(1)}$)$_{1.7(1)}$Fe$_2$Se$_2$ carries large uncertainties due to intrinsic disorder in the material, large displacement ellipsoids and significant parameter correlations resulting from the limited Q-range at high Q available on WISH. The less-than-full nitrogen site occupancy is consistent with the volumetric absorption of ammonia (see below) and a refined D:N ratio less than 3 is consistent with the ammonia-poor material containing some amide moieties.[8] The Fe–Se distances of 2.415(1) Å and the Se–Fe–Se angles of 103.65(3)° (× 2) and 112.46(2)° (× 4) are very similar to the values in the ammonia-poor intercalate at 8 K (Se–Fe–Se bond angles of 104.40(8)° (× 2) and 112.06(4)° (× 4) and Fe–Se bonds of 2.408(1) Å, consistent with a non-redox intercalation of further ammonia. The ammonia and amide moieties are modelled as orientationally disordered and there are N–D···Se hydrogen bonds with a D···Se separation of 2.756(4) Å, similar to that in the ammonia-poor intercalates (2.761(3) Å).[8] The freely refined N–D distances of 0.955(4) and 0.884(5) Å and the D···N separation of 2.719(5) Å between adjacent ND$_3$ molecules and the Li–N distances of 2.1837(6) Å are comparable to the distances found in solid ND$_3$ (N–D of 1.012(2) Å and D···N intermolecular distance of 2.357(2) Å at 2 K),[15] LiND$_2$ (Li–N of 2.065(3)–2.210(3) Å, N–D of 0.967(5) and 0.978(6) Å)[16] and Li(ND$_3$)$_4$ (Li–N of 2.035(5)–2.078(5) Å and N–D mean of 0.99 Å).[17]

The orientation of the ammonia molecules relative to the selenide and lithium ions is qualitatively similar to the arrangement in the hydrated superconducting phase of Na$_{0.3}$CoO$_2$·1.2D$_2$O ($T_c = 4.5$ K), described in detail by Jorgensen *et al.*[18] That compound also contains a double layer of small polar molecules which in that case separates sodium ions from the transition-metal-containing layers. In both systems there is hydrogen bonding between the hydrogen atoms of the small molecule and the anion of the transition metal layers, and the hydrogen atoms located towards the centre of the intercalate layer avoid the positively charged alkali metal ion.

To probe further the reversible sorption of ammonia by the ammonia-poor Li/ammonia intercalate, an 8 g portion of the ND$_3$-poor intercalate was placed in a steel pressure cell, briefly evacuated and then placed in a closed-cycle refrigerator on WISH. The sample was cooled to 250 K and, with PND data collected continuously, was exposed firstly to a constant 1 atm of ND$_3$ and secondly to a 500 cm^3 buffer volume of ND$_3$ initially at 1 atm. In both cases the sample was observed to absorb ND$_3$ extremely rapidly with 90 % of the ND$_3$ absorbed from the buffer volume within 45 min, consistent with the refined composition. Between these two charging experiments the sample was exposed to a dynamic vacuum at 260 K and was observed to desorb all the additional ND$_3$, to regenerate the ND$_3$-poor intercalate. The evolution of the neutron diffractograms is shown in Figure 4.
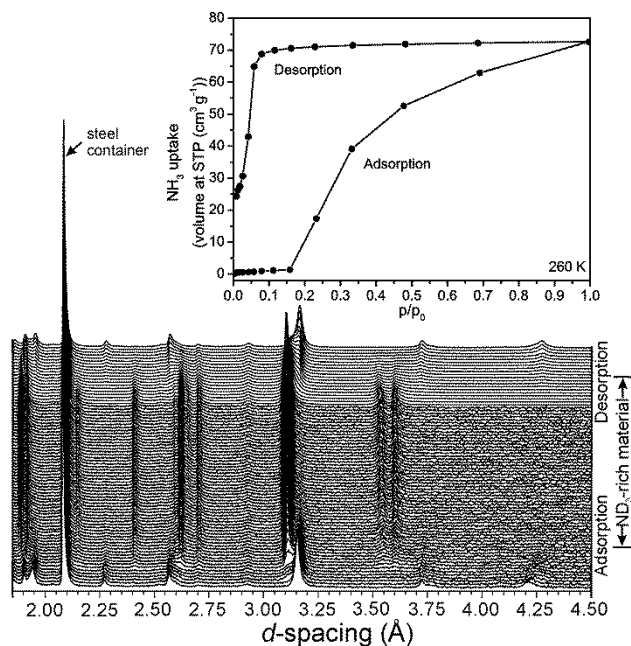

Figure 4. (top):NH$_3$ adsorption and desorption isotherms for the ammonia-poor intercalate. (bottom): PND patterns (WISH) during adsorption and desorption of ND$_3$ by the ammonia-poor intercalate at 250 K. The phases present are the ND$_3$-poor and ND$_3$-rich intercalates and the steel container.

The NH$_3$ adsorption isotherm at 260 K was subsequently measured on 1.039 g (= 3.575 mmol) of NH$_3$-poor Li/NH$_3$ intercalate (Figure 4, top) with an automated gas sorption analyzer (QUANTACHROME Autosorb iQ). The uptake of NH$_3$ of 72.6 cm^{3}g^{-1} corresponds to the adsorption of about 0.9 moles of NH$_3$ per mole of Li$_{0.6}$(NH$_{2.8}$)Fe$_2$Se$_2$[8] at 1 atm (theoretical value: 79.0 cm^{3}g^{-1}), supporting the conclusions of the PND measurements that ammonia molecules do not fill all the available crystallographic sites under the synthetic conditions. The isotherm shows rapid adsorption of NH$_3$ once the NH$_3$ pressure reaches 0.2 atm, and the isotherm is hysteretic with appreciable desorption of NH$_3$

at 260 K only occurring when the pressure is reduced to 0.1 atm above the solid. This profile is typical for inter-lamellar intercalation of polar molecules as described by Barrer.[19] The intercalation and deintercalation of NH_3 into sodium montmorillonite[20] is strikingly similar to the adsorption and desorption behaviour in our case. This isotherm helps to quantify the tendency of the ammonia-rich intercalates to desorb half of their ammonia and explains why the normal use of a Schlenk line (evacuation of the sample container at ambient temperatures) does not enable these materials to be observed easily.

Magnetometry on a sample of the material synthesised using similar apparatus to that used for the *in-situ* PXRD measurements and maintained suspended in liquid or frozen ammonia (see ESI) revealed a bulk superconductor with a T_c of 39(1) K (Figure 5), about 5 K lower than for the ammonia-poor intercalates.[7,8] A second sample prepared by exposing the ammonia-poor intercalate to 1 atm of NH_3 at −10°C (replicating closely the synthesis of the sample used in the PND experiment and the adsorption experiment) yielded a similar T_c. The superconducting volume fractions are estimated to be 30-40% by comparison with the ammonia-poor intercalates.[8]
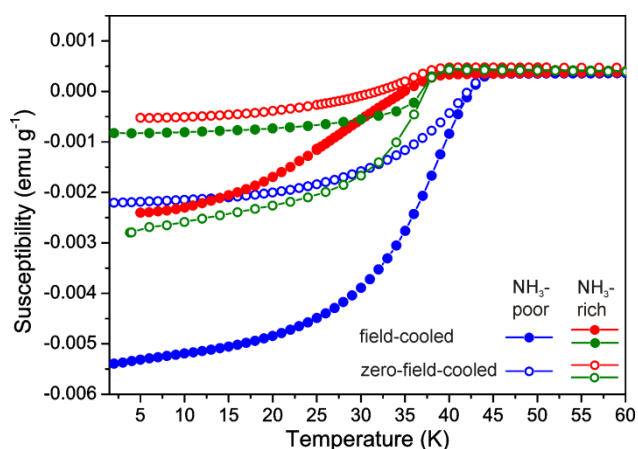

Figure 5. The magnetic susceptibilities of: an ammonia-rich intercalate (green) suspended frozen in some of the ammonia used in its synthesis (see ESI); an ammonia-rich intercalate (red) synthesised by exposing the ammonia-poor intercalate (blue) to 1 atm of gaseous ammonia at −10°C.

The behaviour of the metal/ammonia intercalates of FeSe is strongly reminiscent of the behaviour of the hydrates of $Na_{0.3}CoO_2$.[21,22] The ammonia-rich phase identified here corresponds to the hydrated superconductor $Na_{0.3}CoO_2 \cdot 1.2H_2O$[18,21] and the ammonia-poor material described previously[8] corresponds to non-superconducting $Na_{0.3}CoO_2 \cdot 0.6H_2O$.[22] The cobaltates have hexagonal CoO_2 layers composed of edge-linked CoO_6 octahedra, while the iron selenides have tetragonal layers composed of edge-linked $FeSe_4$ tetrahedra. In the iron selenide system, ammonia-free $K_{0.3}Fe_2Se_2$ corresponding to $Na_{0.3}CoO_2$, has been reported by Ying *et al.* prepared by de-ammoniation at 200 °C,[12] and the composition $M_xFe_2Se_2$ (M = K, Rb; x estimated as 0.3–0.5)[10,11] appears to be a 33 K superconductor which often co-exists as a minor phase intergrown with iron-deficient antiferromagnetic Mott-Hubbard insulators with compositions close to $M_{0.8}Fe_{1.6}Se_2$ synthesised at high temperatures.[11] In the case of the ammonia-poor Li/NH_3 intercalate of iron selenide, removal of further ammonia is facile, but is accompanied by reduction of iron to the element and eventual formation of Li_2Se.[8]

The investigations described here not only expand the range of iron-based high temperature superconductors and promise further molecular intercalates, but also underline how rapid data collection from modern diffractometers allows otherwise fleeting phases to be identified, targeted and characterized.

ASSOCIATED CONTENT

Supporting Information

Further experimental details, including safety instructions and further diffractograms and experimental data are provided as supporting information. This material is available free of charge via the Internet at http://pubs.acs.org."

AUTHOR INFORMATION

Corresponding Author

Simon J Clarke, simon.clarke@chem.ox.ac.uk.

Notes

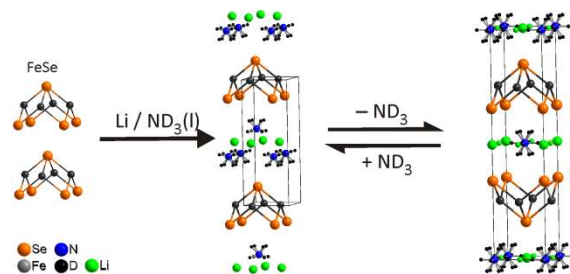The authors declare no competing financial interests.

ACKNOWLEDGMENT

REFERENCES

1. Sefat, A. S. *Curr. Opin. Solid State Mater. Sci.* **2013**, *17*, 59.

2. Johrendt, D. *J. Mater. Chem.* **2011**, *21*, 13726.

3. Fujitsu, S.; Matsuishi, S.; Hosono, H. *Int. Mater. Rev.* **2012**, *57*, 311.

4. Hirschfeld, P. J.; Korshunov, M. M.; Mazin, I. I. *Rep. Prog. Phys.* **2011**, *74*, 124508.

5. Hsu, F.-C.; Luo, J.-Y.; Yeh, K.-W.; Chen, T.-K.; Huang, T.-W.; Wu, P. M.; Lee, Y.-C.; Huang, Y.-L.; Chu, Y.-Y.; Yan, D.-C.; Wu, M.-K. *Proc. Natl. Acad. Sci.* **2008**, *105*, 14262.

6. McQueen, T. M.; Huang, Q.; Ksenofontov, V.; Felser, C.; Xu, Q.; Zandbergen, H.; Hor, Y. S.; Allred, J.; Williams, A. J.; Qu, Q.; Checkelsky, J.; Ong, N. P.; Cava, R. J. *Phys. Rev. B: Condens. Mater. Phys.* **2009**, *79*, 014522.

7. Ying, T. P.; Chen, X. L.; Wang, G.; Jin, S.F.; Zhou, T. T.; Lai, X. F.; Zhang, H.; Wang, W. Y. *Sci. Rep.* **2012**, *2*, 426.

8. Burrard-Lucas, M.; Free, D. G.; Sedlmaier, S. J.; Wright, J. D.; Cassidy, S. J.; Hara, Y.; Corkett, A. J.; Lancaster, T.; Baker, P. J.; Blundell, S. J.; Clarke, S. J. *Nat. Mater.* **2013**, *12*, 15.

9. Scheidt, E.-W.; Hathawar, V. R.; Schmitz, D.; Dunbar, A.; Scherer, W.; Mayr, F.; Tsurkan, V.; Deisenhofer, J.; Loidl, A. *Eur. Phys. J. B.* **2012**, *85*, 279.

10. Texier, Y.; Deisenhofer, J.; Tsurkan, V.; Loidl, A.; Inosov, D. S.; Friemel, G.; Bobroff, J. *Phys. Rev. Lett.* **2012**, *108*, 237002.

11. Shoemaker, D. P.; Chung, D. Y.; Claus, H.; Francisco, M. C.; Avci, S.; Llobet, A.; Kanatzidis, M. G. *Phys. Rev. B: Condens. Mater. Phys.* **2012**, *86*, 184511.

12. Ying, T.; Chen, X.; Wang, G.; Jin, S; Lai, X.; Zhou, T.; Zhang, H.; Shen, S.; Wang, W. *J. Am. Chem. Soc.* **2013**, *135*, 2951.

13. Williams, G. R.; O'Hare, D. *Chem. Mater.* **2005**, *17*, 2632.

14. Coelho, A. A. TOPAS Academic, Version 5; Coelho Software, Brisbane, Australia, **2012**.

15. Hewat, A. W.; Riekel, C. *Acta Crystallogr. A* **1979**, *35*, 569.

16. Sørby, M. H.; Nakamura, Y.; Brinks, H. W.; Ichikawa, T.; Hino, S.; Fujii, H.; Hauback, B.C. *J. Alloys Compd.* **2007**, *428*, 297.

17. Ibberson, R. M.; Fowkes, A. J.; Rosseinsky, M. J.; David, W. I. F.; Edwards, P. P. *Angew. Chem. Int. Ed.* **2009**, *48*, 1435.

18. Jorgensen, J. D.; Avdeev, M.; Hinks, D. G.; Burley, J. C.; Short, S. *Phys. Rev. B: Condens. Mater. Phys.* **2003**, *68*, 214517.

19. Barrer, R. M. *Pure & Appl. Chem.* **1989**, *61*, 1903.

20. Barrer, R. M.; MacLeod, D. M. *Trans. Faraday Soc.* **1954**, *50*, 980.

21. Takada, K.; Sakurai, H.; Takayama-Muromachi, E.; Izumi, F.; Dilanian, R. A.; Sasaki, T. *Nature* **2003**, *422*, 53.

22. Takada, K.; Sakurai, H.; Takayama-Muromachi, E.; Izumi, F.; Dilanian, R. A.; Sasaki, T. *J. Solid State Chem.* **2004**, *177*, 372.

SYNOPSIS TOC (Word Style "SN_Synopsis_TOC"). If you are submitting your paper to a journal that requires a synopsis graphic and/or synopsis paragraph, see the Instructions for Authors on the journal's homepage for a description of what needs to be provided and for the size requirements of the artwork.

Authors are required to submit a graphic entry for the Table of Contents (TOC) that, in conjunction with the manuscript title, should give the reader a representative idea of one of the following: A key structure, reaction, equation, concept, or theorem, etc., that is discussed in the manuscript. Consult the journal's Instructions for Authors for TOC graphic specifications.

Ammonia-rich high temperature superconducting intercalates of iron selenide revealed through time-resolved *in-situ* X-ray and neutron diffraction.

Stefan J Sedlmaier,[1] Simon J Cassidy,[1,2] Richard G Morris,[1] Michael Drakopoulos,[2] Christina Reinhard,[2] Saul J Moorhouse,[1,2] Dermot O'Hare,[1] Pascal Manuel,[3] Dmitry Khalyavin[3] and Simon J Clarke[1*]

[1]*Department of Chemistry, University of Oxford, Inorganic Chemistry Laboratory, South Parks Road, Oxford, OX1 3QR, UK.* [2]*Diamond Light Source Ltd., Harwell Science and Innovation Campus, Didcot, OX11 0DE, UK .*[3]*ISIS Facility, STFC Rutherford Appleton Laboratory, Harwell Oxford, Didcot OX11 0QX, United Kingdom.*

Supporting Information

1. Experimental set-up on the Joint Engineering, Environmental and Processing (JEEP) beamline I12
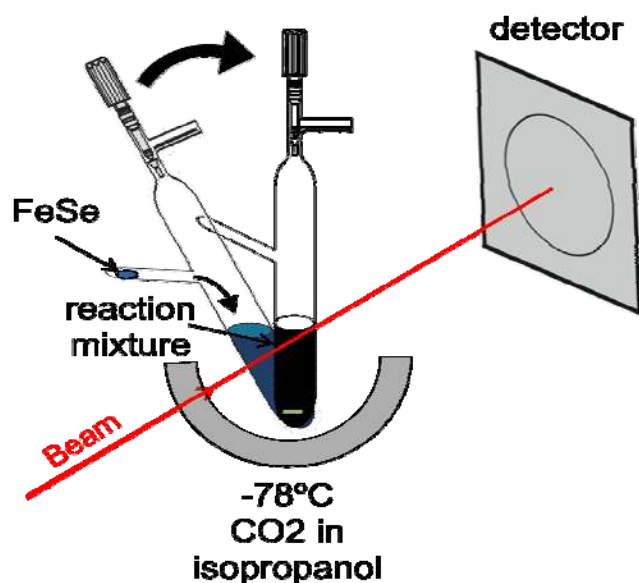
Figure S1. Schematic of the *in-situ* experiment carried out on I12. The ampoule was rotated by a remote-controlled rotation stage while the solution was exposed to the beam and the FeSe was tipped into the solution.

2. Safety precautions of the ampoules

The ampoules were constructed from pyrex glass with an outer diameter of 18 mm and a wall thickness of 4 mm (12 mm × 3 mm for the side arm, see Figure S5) equipped with High Performance Rotaflo® teflon valves. Overall the ampoules were conservatively rated to pressures approximately double the sum of the autogenous pressure generated by ammonia at room temperature and the hydrogen pressure that would be generated assuming complete decomposition of the Li/NH$_3$ solution.

3. Single diffractograms measured running a Li/NH$_3$ + FeSe reaction on I12 with a exposure time of 80 ms
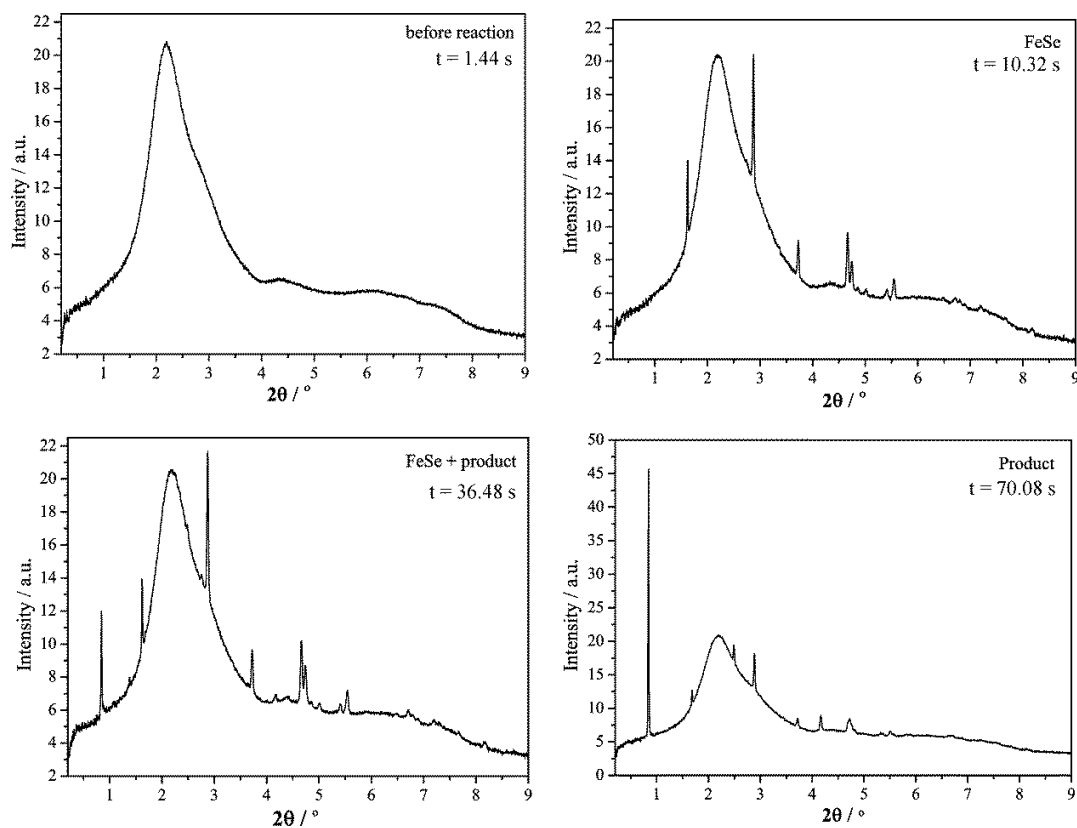

Figure S2. The four diffractograms show the reaction of a Li/NH$_3$ solution with FeSe at different times t. As verified with empty measurements, the background arises from the sample environment (thick wall glass ampoule, dewar, solution, air etc.). Bragg peaks due to FeSe appear immediately after the powder is poured into the solution and the product progressively appears. These diffractograms were each collected in 80ms at room temperature.

4. Results of refinements against I12 X-ray diffraction data

Table S1. Crystallographic data for (Li)FeSeN (esd's in parentheses)

Crystal Structure Data	
formula	FeSeN
formula mass / gmol^{-1}	148.812
crystal system	tetragonal
space group	*P4/nmm* (no. 129, origin choice 2)
cell parameters / Å	$a = 3.82766(8)$
	$c = 10.5938(7)$
cell volume / Å^3	$V = 155.210(12)$
formula units Z / cell	2
X-ray density ρ / g·cm^{-3}	3.1842(3)
Data collection	
diffractometer / radiation	I12 Diamond, $\lambda = 0.156$ Å
temperature / K	297(2)
2θ range / °	0.4 - 9.5
data points	1914
number of reflections	82
Structure Refinement	
method of refinement	Rietveld, fundamental parameters model[1]
program used	TOPAS-Academic V5[2]
total number of parameters	65
background function / parameters	shifted Chebyshev / 44
number of atomic parameters	5
number of profile and other parameters	16
R indices	$R_p = 0.00297$
	$wR_p = 0.00409$
	$R_{Bragg} = 0.00124$

Table S2. Atomic coordinates, Wyckoff symbols, occupancy and isotropic displacement parameters B_{eq} (Å^2) for the atoms in (Li)FeSeN (esd's in parentheses)

atom	Wyckoff symbol	x	y	z	occupancy	B_{eq}
Se	2c	¼	¼	0.13808(26)	1	1.76(12)
Fe	2a	¾	¼	0	1	0.64(9)
N	2c	¾	¾	0.39714(100)	1†	1.74(40)

† data quality is insufficient to attempt to refine a reliable occupancy of N; so it was set to 1.
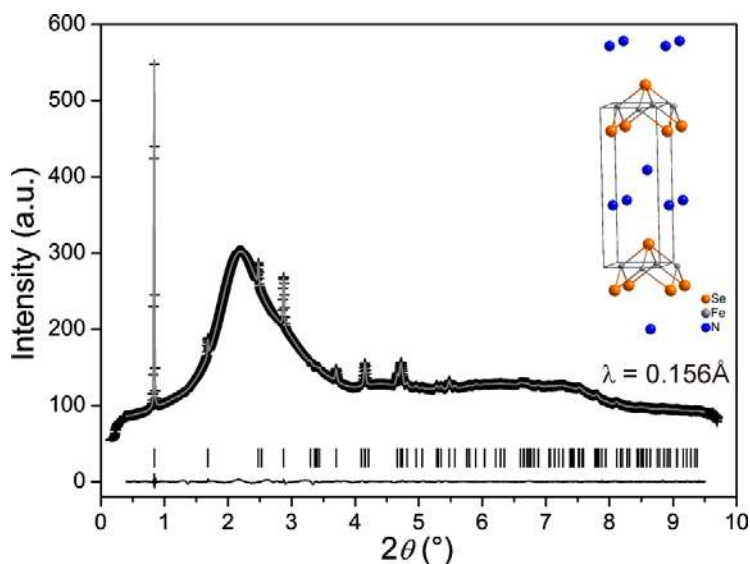
Figure S3. Observed (crosses) and calculated (gray line) powder diffraction pattern of the final product of a reaction of Li/NH$_3$ with FeSe suspended in NH$_3$ as well as difference profile of the Rietveld refinement; peak positions are marked by vertical lines.
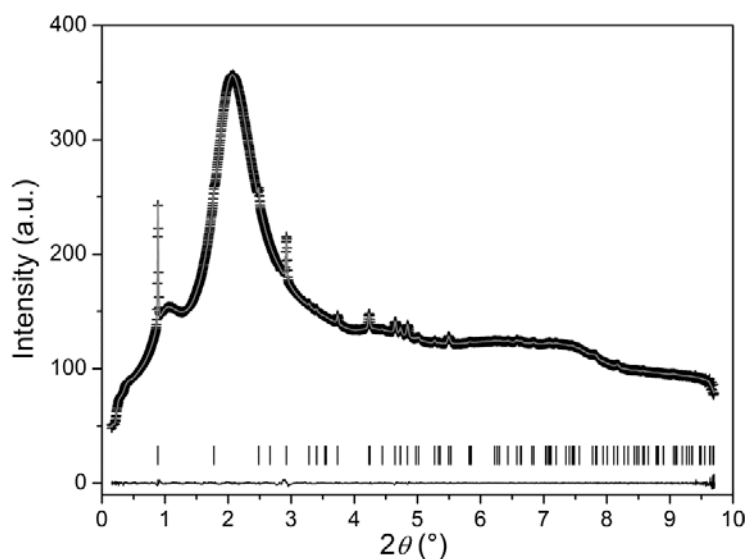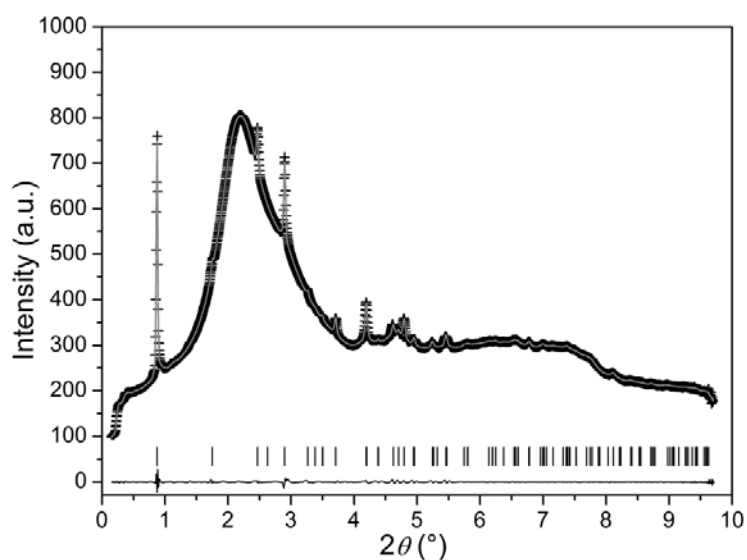

Figure S4. Observed (crosses) and calculated (gray line) powder diffraction pattern of the final product of a reaction of Rb/NH$_3$ with FeSe (Rb/FeSe ratio = 0.5) suspended in NH$_3$ as well as difference profile of the Pawley refinement (a model independent refinement against the diffraction profile implemented within the TOPAS academic software[2]); peak positions are marked by vertical lines.

Figure S5. Observed (crosses) and calculated (gray line) powder diffraction pattern of the final product of a reaction of K/NH$_3$ with FeSe (K/FeSe ratio = 0.15) suspended in NH$_3$ as well as difference profile of the Pawley refinement; peak positions are marked by vertical lines.
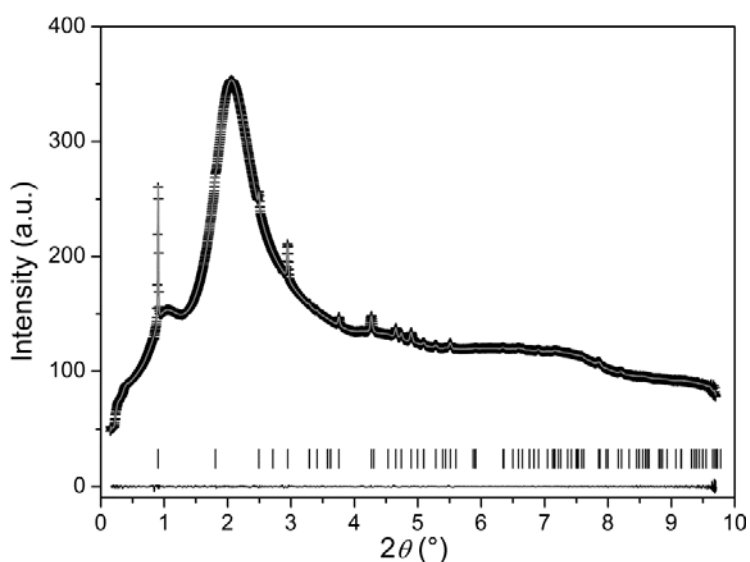

Figure S6. Observed (crosses) and calculated (gray line) powder diffraction pattern of the final product of a reaction of K/NH$_3$ with FeSe (K/FeSe ratio = 0.3) suspended in NH$_3$ as well as difference profile of the Pawley refinement; peak positions are marked by vertical lines.

5. Results of the structure refinement against WISH neutron diffraction data for the ammonia-rich Li/ammonia intercalate.

Table S3. Crystallographic data for $Li_{0.56(1)}N_{1.72(2)}D_{4.63(3)}Fe_2Se_2$ (esd's in parentheses)

Crystal Structure Data	
formula	$Li_{0.28(1)}N_{0.86(1)}D_{2.32(2)}FeSe$
formula mass / $gmol^{-1}$	153.457
crystal system	tetragonal
space group	*P4/nmm* (no. 129, origin choice 2)
cell parameters / Å	$a = 3.79756(2)$
	$c = 10.30704(8)$
cell volume / $Å^3$	$V = 148.643(2)$
formula units Z / cell	2
X-ray density ρ / $g \cdot cm^{-3}$	3.376(3)
Data collection	
diffractometer / radiation	WISH (ISIS), TOF (1.5 – 15 Å)
temperature / K	5(1)
data points	17367 (5 datasets)
number of reflections	627
Structure Refinement	
method of refinement	Rietveld
program used	TOPAS-Academic V5[2]
total number of parameters	203
background function / parameters	shifted Chebyshev / 116
number of structural parameters	17
number of profile and other parameters	70
R indices	$R_p = 0.02044$
	$wR_p = 0.01794$
	$R_{Bragg} = 0.00605$

Table S4. Atomic coordinates, Wyckoff symbols, occupancy and isotropic displacement parameters B_{eq} (Å^2) for the atoms in $\text{Li}_{0.56(1)}\text{N}_{1.72(2)}\text{D}_{4.63(3)}\text{Fe}_2\text{Se}_2$ (esd's in parentheses). Space group $P4/nmm$ (origin choice 2).

atom	Wyckoff symbol	x	y	z	occupancy	B_{eq}
Se	2c	¼	¼	0.14485(7)	1	0[†]
Fe	2a	¾	¼	0	1	0[†]
N	2c	¼	¼	0.60678(14)	0.859(9)	0.45(7)
D1	8j	0.1262(9)	0.1262(9)	0.6732(4)	0.282(3)	-
D2	8j	0.0889(9)	0.0889(9)	0.5892(6)	0.297(4)	5.81(10)[‡]
Li	2b	¾	¼	½	0.278(5)	0.45(7)

† as the thermal motion of Se and Fe at 5 K can be assumed to be very low B_{eq} of Se and Fe were set to 0.
‡ as the anisotropic displacement ellipsoid of D2 almost refined to a isotropic shape and to save structural parameters, B_{eq} of D2 was restrained to U_{eq} of D1 ($B_{eq}(\text{D2}) = 1/3(U11+U22+U33)8\pi^2$)

Table S5. Anisotropic displacement parameters U_{ij} (100 Å^2) for the atoms in $\text{Li}_{0.56(1)}\text{N}_{1.72(2)}\text{D}_{4.63(3)}\text{Fe}_2\text{Se}_2$ (esd's in parentheses)

	U_{11}	U_{22}	U_{33}	U_{12}	U_{13}	U_{23}
D1	9.45(16)	9.45(16)	3.2(3)	-5.5(3)	2.63(12)	2.63(12)

Table S6. Selected interatomic distances (Å) and angles (°) in $\text{Li}_{0.56(1)}\text{N}_{1.72(2)}\text{D}_{4.63(3)}\text{Fe}_2\text{Se}_2$ (e.s.ds. in parentheses)

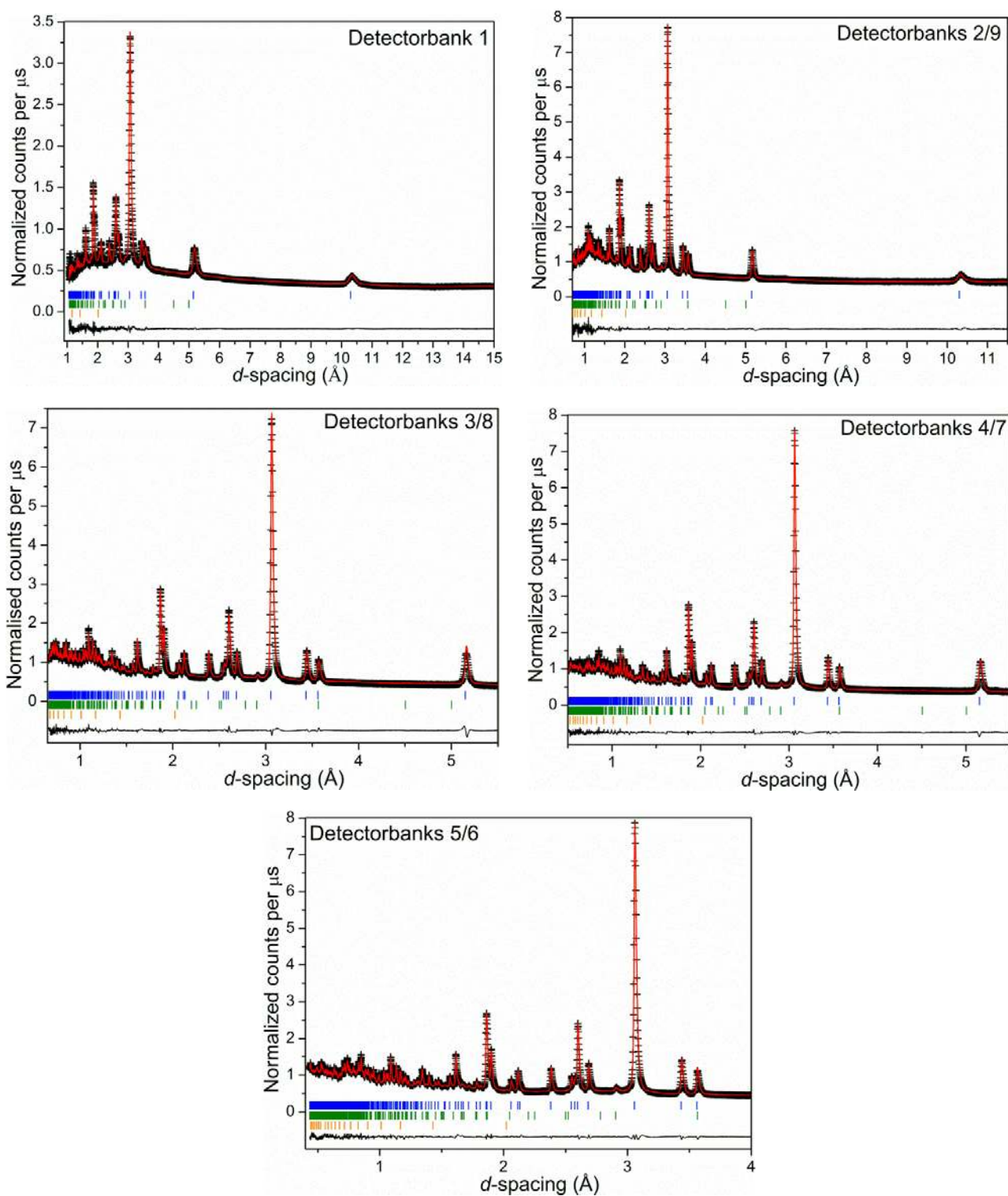|	
Fe–Se	2.4154(4)
Se–Fe–Se	103.65(3), 112.460(14)
Li–N	2.1947(7)
N–D	0.955(4) (D1), 0.884(5) (D2)
N···Se	3.7100(11)
D1···Se	2.756(4)
N–D1···Se	177.0(3)

Figure S7. Observed (crosses) and calculated (red lines) neutron powder diffraction patterns as well as difference profiles of the Rietveld refinements of the ammonia-rich Li/NH$_3$ intercalate against WISH data at 5 K; peak positions are marked by blue (main phase), green (LiNH$_2$ impurity, 0.2 weight%) and orange (iron impurity, 0.4 weight%) vertical lines.
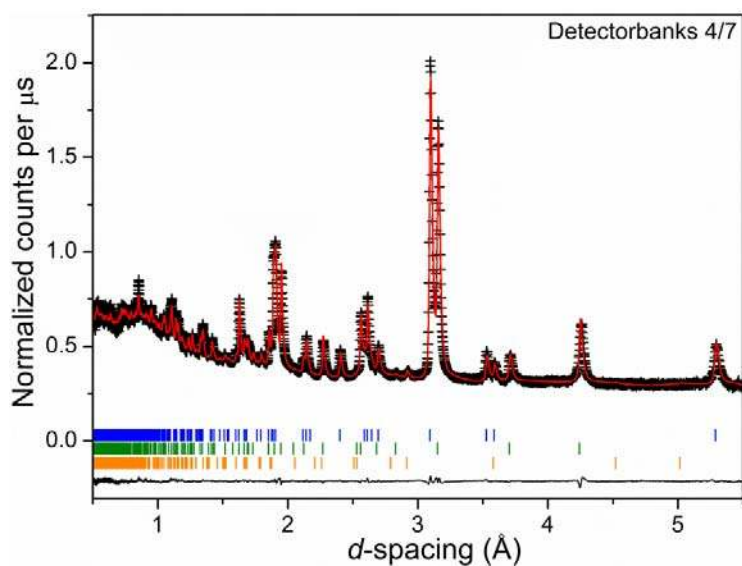
Figure S8. Observed (black crosses) and calculated (red line) neutron powder diffraction patterns as well as the difference profile of the Rietveld refinement against WISH data of a ammonia-poor Li/ND_3 intercalate sample exposed to ND_3 0°C for 4 h conducted at 270 K; peak positions are marked by blue (ammonia-rich Li/FeSe intercalate, 41.8 weight%), orange (ammonia-poor Li/FeSe intercalate, 58.1 weight %) and green ($LiNH_2$ impurity, 0.1 weight%) vertical lines.

6. Preparation of a sample for magnetometry

Figure S9. Apparatus for handling the ammonia-rich solid in liquid ammonia. The ratio of the glass wall thickness to the overall diameter must be chosen to ensure that the autogenous pressure of ammonia does not rupture the tube. E.g. 18 mm o.d. × 4mm wall for the reaction tube shown left (similar to that used on I12) or 5mm o.d. × 1 mm wall for the spur sealed off for the magnetometry measurements (right). Refer to the glass supplier's data and use a professional glassblower to construct the apparatus.

7. Analysis of the reactions of Li/NH₃ and FeSe run on I12

This section contains the film plots of the Li/NH$_3$/FeSe reactions run at different temperatures. In addition to that it contains plots of the integrated intensities of the (001) reflections of FeSe and the product suspended in NH$_3$ normalised to 1 against time to get an idea of the progress of the reactions. It is assumed that a constant amount of powder is in the beam at all times.
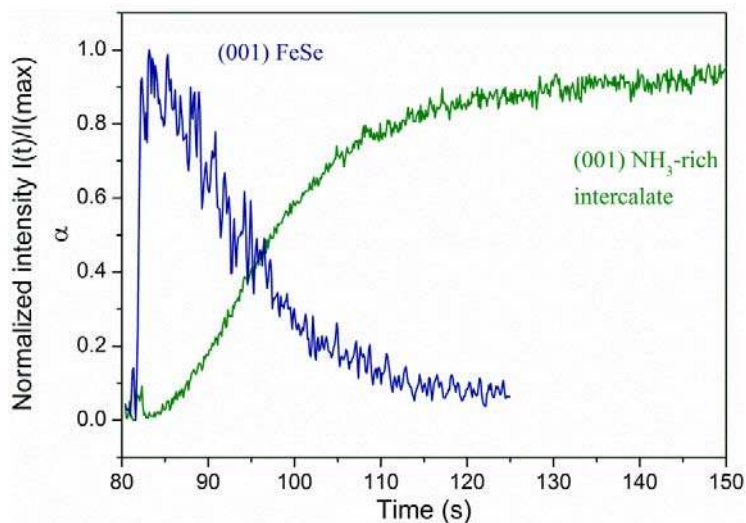

Figure S10. Evolution of the integrated normalized intensities of the (001) reflections of the starting material FeSe and the NH$_3$-rich product running a reaction of Li/NH$_3$ solution with FeSe at RT; 80 ms exposure time per image (40 ms dead time); related film plot is displayed as Figure 2a in the main article.
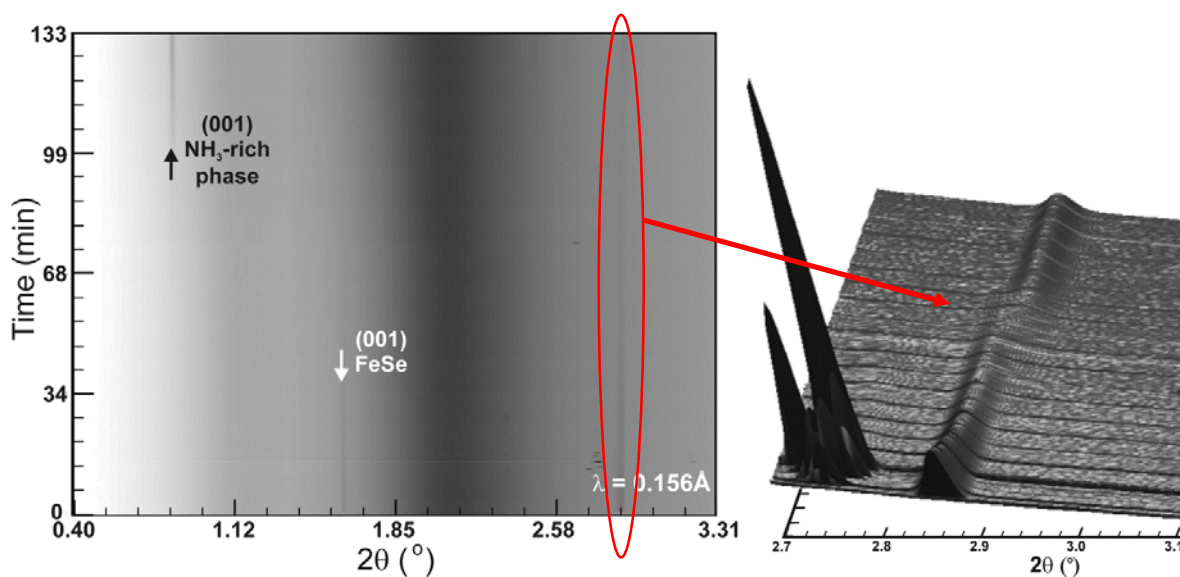
Figure S11. Film plot showing the evolution of the diffraction patterns measured on I12 when FeSe was added to Li/NH$_3$ solution at −78°C; the evolution of the (011) reflection ((012) in the final pattern) showing a slight shift and minimum in

cristallinity is shown on the left (the block of peaks on the left in this part of the figure with random intensity are due to sample environment – solid CO_2 or stirrer bar).
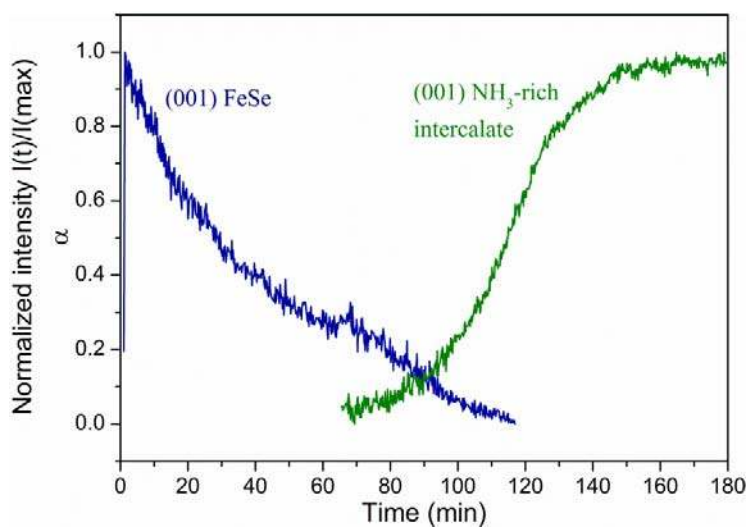

Figure S12. Evolution of the integrated normalized intensities of the (001) reflections of the starting material FeSe and the NH_3-rich product running a reaction of Li/NH_3 solution with FeSe at −78°C; 4 s exposure time per image (1 s dead time).
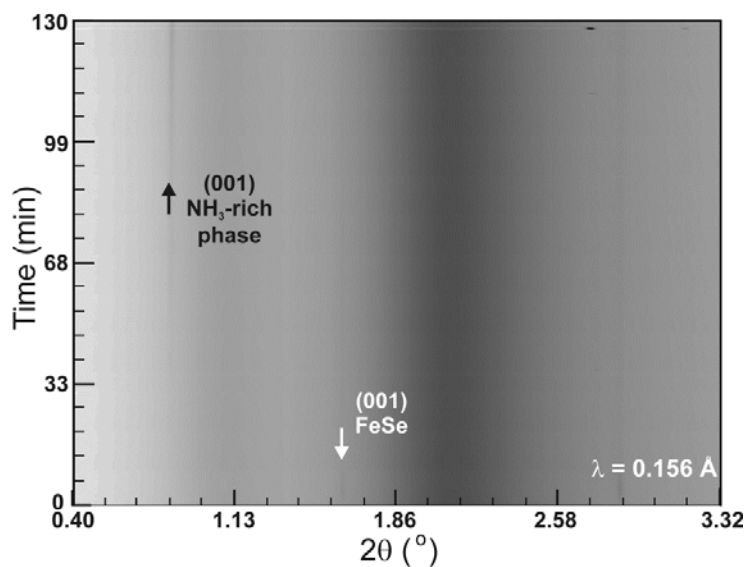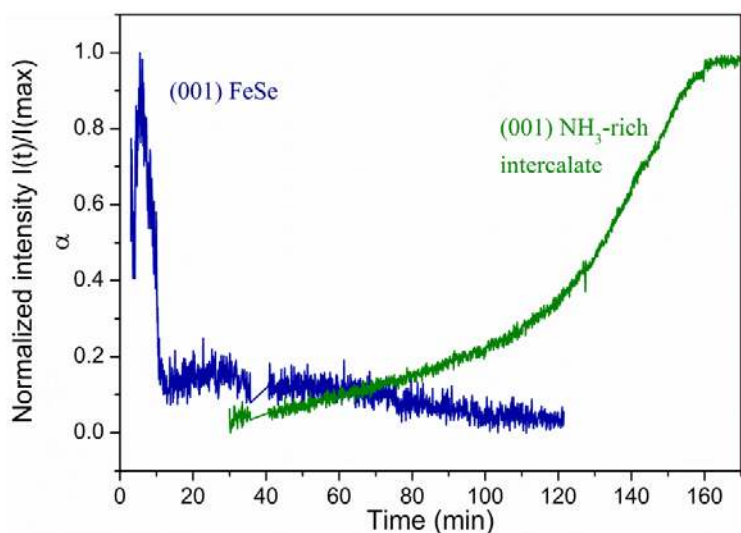

Figure S13. Film plot showing the evolution of the diffraction patterns measured on I12 when FeSe was added to Li/NH_3 solution at −78°C.

Figure S14. Evolution of the integrated normalized intensities of the (001) reflections of the starting material FeSe and the NH$_3$-rich product running a reaction of Li/NH$_3$ solution with FeSe at −78°C; 4 s exposure time per image (1 s dead time); this measurement includes a break in measurement of 5 min after 34 min.
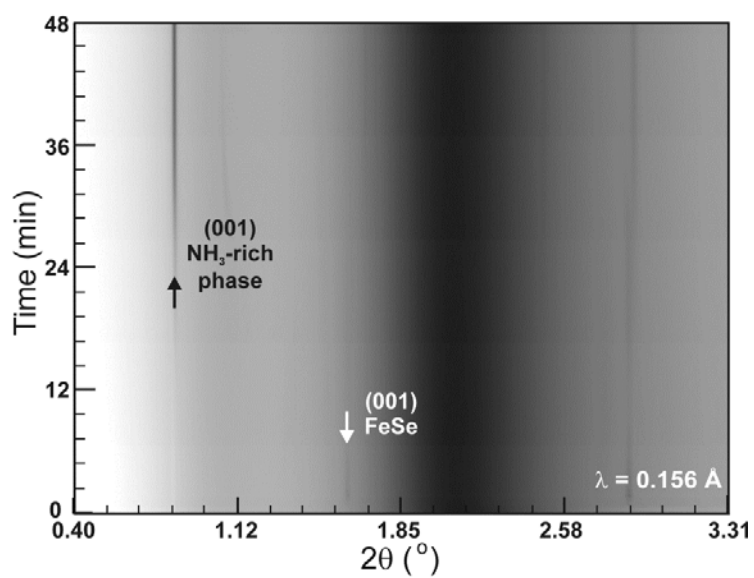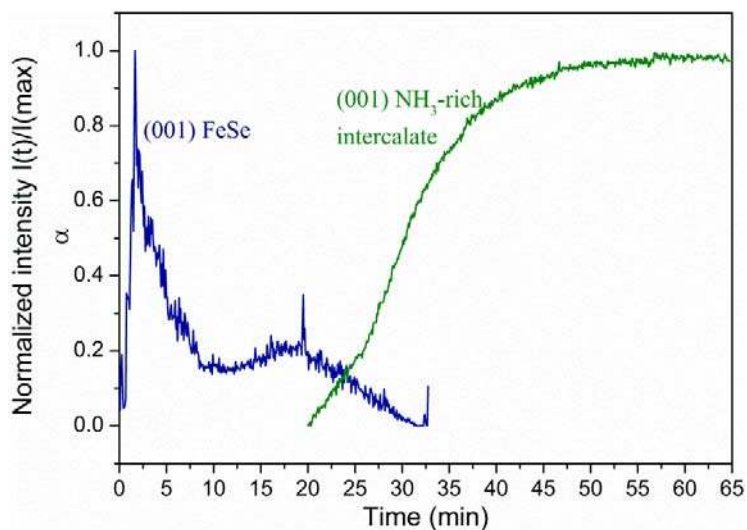

Figure S15. Film plot showing the evolution of the diffraction patterns measured on I12 when FeSe was added to a Li/NH$_3$ solution at −58°C.

Figure S16. Evolution of the integrated normalized intensities of the (001) reflections of the starting material FeSe and the NH$_3$-rich product running a reaction of Li/NH$_3$ solution with FeSe at −58°C; 4 s exposure time per image (1 s dead time).
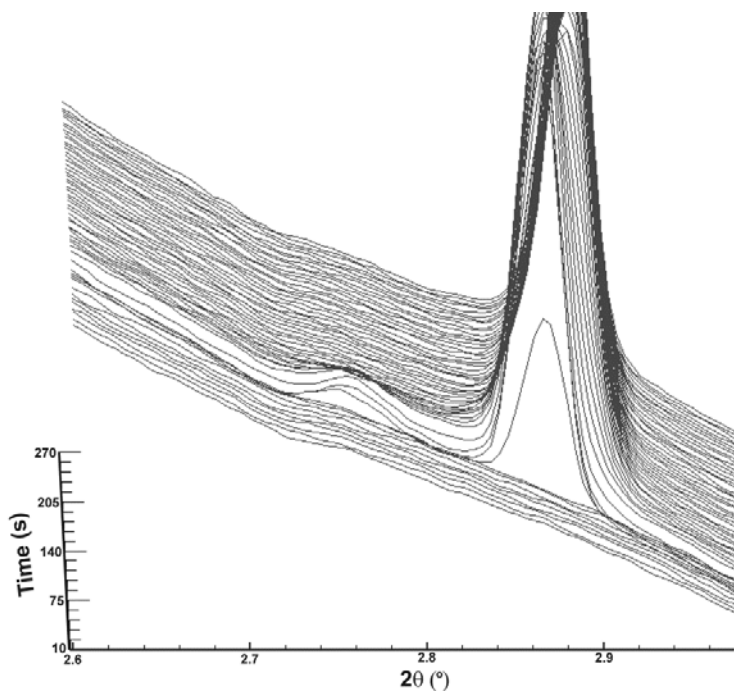

Figure S17. Appearance and disappearance of a weak reflection at around 2θ = 2.75º (d = 3.26 Å) during the reaction of the Li/ammonia solution with FeSe at room temperature suggesting an intermediate phase.
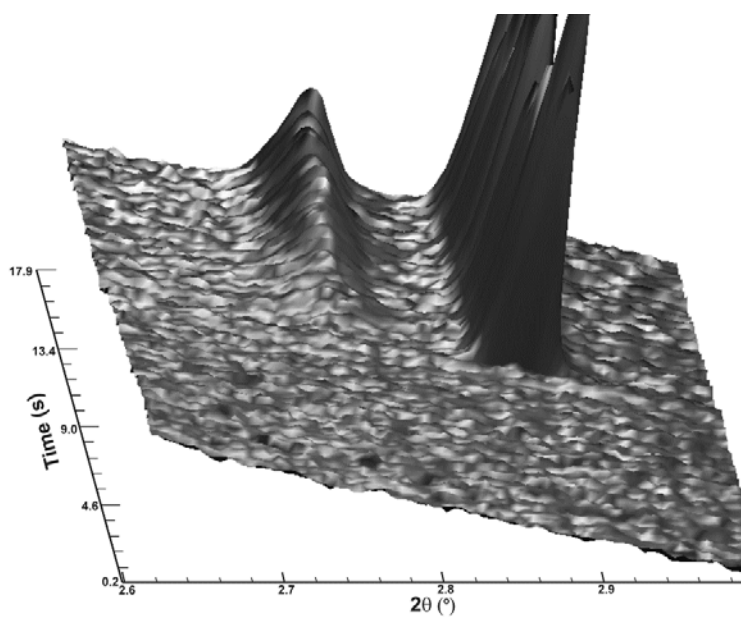
Figure S18. Appearance a weak reflection at around $2\theta = 2.75°$ ($d = 3.26$ Å) during the reaction of the Li/ammonia solution with FeSe at room temperature suggesting an intermediate phase; disappearance of this could not be observed due to loss of communication with the detector during this particular run, however the reflection is not present in the final diffraction pattern.

8. References

[1] Bergmann, J.; Kleeberg, R.; Haase, A.; Breidenstein, B. *Mat. Sci. Forum* **2000**, *347-349*, 303-308.
[2] A. A. Coelho, *TOPAS-Academic,* Version V5, Coelho Software, Brisbane, **2012**.